PHYSICAL REVIEW B **107**, 214103 (2023)

Active reconfiguration of multistable metamaterials for linear locomotion

Jiajia Shen,[1,*] Martin Garrad,[2,3] Qicheng Zhang,[4] Olivia Leao,[1] Alberto Pirrera,[1] and Rainer M. J. Groh[1]
[1]*Bristol Composites Institute (BCI), Department of Aerospace Engineering, University of Bristol, Bristol BS8 1TR, United Kingdom*
[2]*Department of Engineering Mathematics, University of Bristol, Bristol BS8 1TR, United Kingdom*
[3]*SoftLab, Bristol Robotics Laboratory, University of Bristol and University of the West of England, Bristol BS8 1TR, United Kingdom*
[4]*Faculty of Science and Engineering, Swansea University, Swansea, SA1 8EN, United Kingdom*

(Received 13 February 2023; revised 5 May 2023; accepted 26 May 2023; published 15 June 2023)

Buckling-driven shape-shifting is increasingly being used in metamaterials to achieve mechanical programmability and novel functionality. Here, we show that the post-buckling response and the ensuing behavior, of lattice metamaterials can be programed through so-called passive and active modal nudging. Numerical continuation is first used to explore exhaustively the bifurcation manifold of a compressed, elastomeric lattice metamaterial. We then tailor the natural postcritical behavior of the metamaterial by judiciously altering the baseline geometry using modal information extracted from the bifurcation landscape (passive modal nudging). Experimental tests verify the effectiveness of the approach. Subsequently, shape change is induced by actively nudging the metamaterial between two stable postcritical states using an embedded actuator, i.e., by changing the local topology of the metamaterial rather than by controlling a global field. Fundamentally, we use passive modal nudging to bias the metamaterial towards one of three possible postcritical states under applied compression and then employ active nudging to switch between different postcritical states. Based on this paradigm, we manufacture and test a crawling soft robot and demonstrate that locomotion through local actuation to switch between two postcritical states is significantly more energy efficient than the alternative strategy of switching between a precritical and a postcritical state through global actuation. Overall, this paper demonstrates the benefits and promise of programming the behavior of soft metamaterials by exploiting principles of bifurcation theory and using tailored imperfections and embedded actuators.

DOI: 10.1103/PhysRevB.107.214103

I. INTRODUCTION

Mechanical metamaterials—human-made structures with homogenized material properties derived from structural topology rather than the constituent materials themselves—are well known for their tailorable and unique properties, such as negative Poisson's ratio [1,2], negative compressibility transitions [3], negative thermal expansion coefficient [4], negative stiffness [5], morphology [6–8], biomimetic properties [9–11], and active response [12–14].

One fruitful approach to design for "exotic" properties is to construct the metamaterial from unit cells that undergo elastic instabilities, whereby a global phase transition can be initiated as a result of local stimuli [15–17]. The resulting nonlinearity and multistability have been exploited to, for example, enable reversible large deformations and programmability [18–20]. However, multistable systems are imperfection sensitive [21,22] and may respond erratically, if not suitably controlled. This paper demonstrates the possibility of programming the behavior of lattice metamaterials by using both passive means (tailoring the geometry via judicial imperfections) and active means (embedded actuation).

Extensive work has been conducted to tailor the postbuckling behavior of lattice metamaterials by introducing specific geometric "imperfections" or "perturbations" into the original, stress-free geometry during fabrication [23]. Janbaz *et al.* [18] developed a design framework to introduce higher order linear buckling modes as geometric imperfections into the original geometry of soft metamaterials. In particular, they achieved a rotational buckling pattern of square lattice metamaterials under axial compression, which can be used as a soft grasping robotic mechanism. However, identifying the combination of modes to yield the desired response through their method required onerous optimization.

Medina *et al.* [19] adopted a "deflated continuation"-based bifurcation analysis [24] to explore the complex postcritical equilibrium manifold of a compressed elastomeric matrix with a square array of circular holes. They then demonstrated that the metamaterial's response could be biased towards a specific stable postbuckling mode by introducing small geometric imperfections of shape affine to that of the target mode.

The methods in Ref. [18] and Ref. [19] are closely related to the general principle of 'modal nudging' introduced by Cox *et al.* [25], whereby geometric perturbations affine to the mode shape of certain stable postbuckling modes are

---

[*] j.shen@bristol.ac.uk

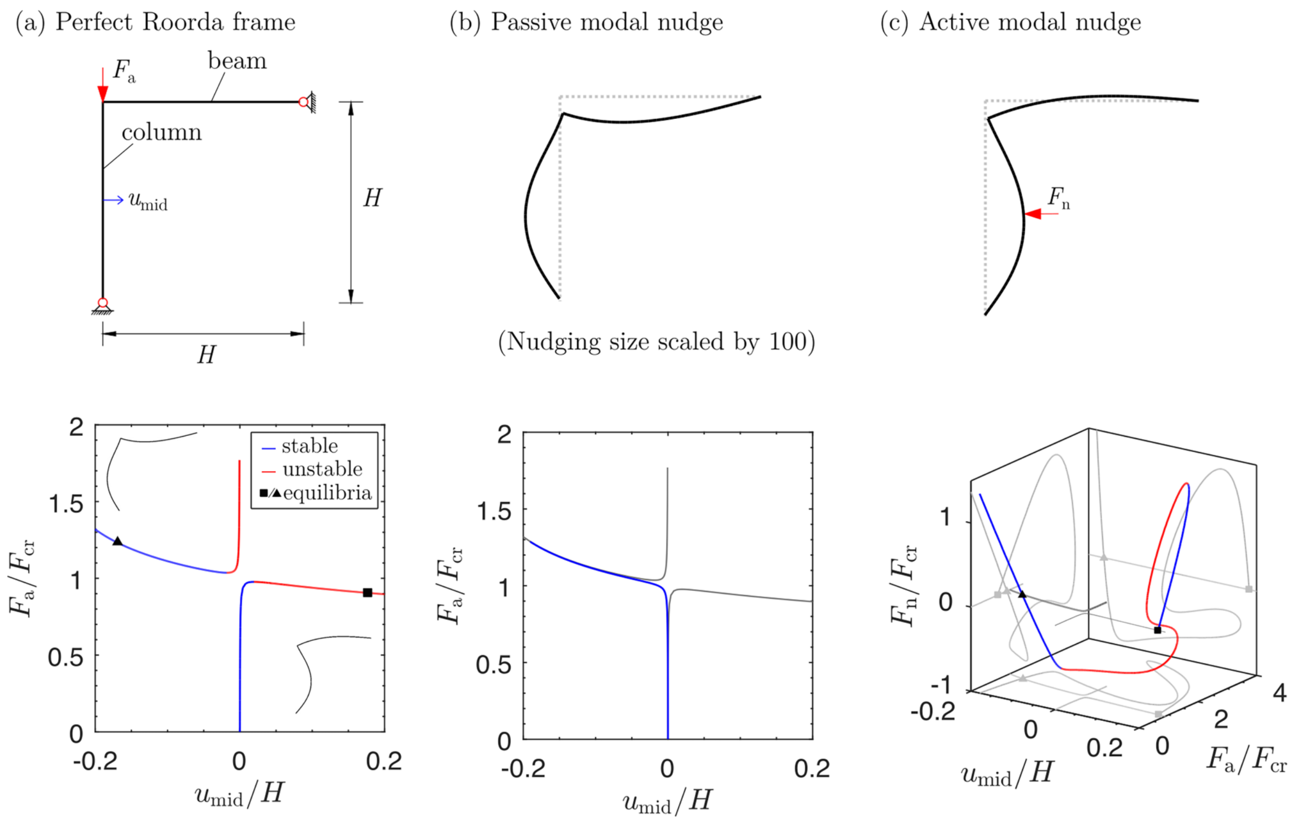

FIG. 1. (a) Perfect Roorda frame [26] under a vertical downwards force at the beam–column junction and the equilibrium path with deformation modes. The column bends rightwards on the natural loading path, and leftwards on the isolated path. Tailored postbuckling behavior using (b) passive and (c) active modal nudging. The equilibrium paths of the perfect Roorda frame are shown in grey. In (b), the frame is nudged with a scaled deformation profile derived from an equilibrium state on the isolated, stable path. In (c), a horizontal force is applied at the mid-height of the column to nudge the Roorda frame from the subcritical branch (solid square) to the supercritical branch (solid triangle).

introduced into the original geometry to alter the natural mechanical behavior. That is, the shape of a disconnected equilibrium, i.e., one on a path in the bifurcation landscape that is separated by an energy barrier from the natural response, can be seeded into the baseline geometry thereby "nudging" the system to spontaneously deform into this otherwise unattainable mode upon loading. A simple example is shown for the well-known Roorda frame [26] in Fig. 1. The vertical column of the Roorda frame naturally prefers to buckle one way due to the presence of the horizontal beam [Fig. 1(a)]. This natural (i.e., spontaneous) predisposition leads to a limit point bifurcation, sudden loss of stability, and collapse of the frame. However, as the response is described by a broken transcritical bifurcation, a broken-away equilibrium branch also exists that is stable and therefore would prevent the loss of stability. Figure 1(b) show that the response of the Roorda frame can be nudged onto this safe path by seeding an initial imperfection—of shape affine to the stable broken equilibrium—that biases the deformation towards the desired mode. In this paper, we use the word "mode" in the colloquial sense to describe a distinguishable deformation modality that corresponds to a certain equilibrium configuration.

Modal nudging requires a method to determine all possible postcritical modes of a structure, i.e., a comprehensive bifurcation analysis that maps out the stability landscape. However, this is beyond the capacities of current commercial finite element packages. Here, we use an in-house nonlinear finite element code with embedded numerical continuation, where isolated broken-away solutions are determined by homotopy [27].

In addition to preprogramming metamaterials using geometric perturbations, efforts have also been made to reprogram metamaterials in the postfabricated state [12,17,28]. With external/internal actuation stimuli, metamaterials can be switched from one stable equilibrium to another, thereby reprogramming the homogenized mechanical properties. The accompanying shape adaption has been exploited for functionality, such as soft actuators [2,19] and information storage [20].

Kidambi *et al.* [29] demonstrated that the behavior of metamaterials can be tailored by boundary forces, but pronounced metastability and energy-releasing state transitions were observed. Additionally, Medina *et al.* [19] showed that the response of lattice metamaterials can be tailored through local manipulation or mechanical restraints. Reprogramming using externally applied fields is also possible. For example, Chen *et al.* [20] developed a reprogrammable metamaterial unit that uses magnetic actuation for mode switching. The metamaterial unit exhibits distinctly different mechanical properties in these two states, i.e., the stiffness and strength can range over an order of magnitude.

To date, tailoring the behavior of metamaterials has largely focused on either passive or active means. However, a more reliable exploitation of metamaterials with many possible postcritical states may be enabled by use of both methods synergistically. Herein, passive modal nudging is used to bias a metamaterial towards one preferred base state in the postcritical regime, thereby overcoming the imperfection sensitivity inherent in multistable systems. Active modal nudging is then used to add functionality by enabling the metamaterial to switch between different stable modes. Crucially, the actuation in active nudging is applied locally to change the local orientation of the "microstructure" of the metamaterial. This contrasts with actuation at the global length scale and significantly reduces the energy required to enable the desired mode switch and the ensuing functionality.

II. METHODS

a. Finite-element formulation and generalized path-following technique. An in-house nonlinear finite element formulation for large deformation (geometric nonlinearity) and finite strain (material nonlinearity) problems is adopted herein, coupled to numerical continuation algorithms. The modeling framework has been described and validated against experimental results in previous work [30,31]. Specifically, a compressible Neo-Hookean hyperelastic model [32] is adopted to describe the material nonlinearity. In the analyses, we reduce the structure to a planar 2D geometry, and enforce the dimensional reduction by assuming a *plane strain* condition in the third dimension. A structured uniform mesh is adopted to discretize the geometry using 16-noded 2D elements.

A generalized path-following solver [27,33] is used to trace nonlinear equilibrium paths based on Riks' arc-length method [34], to pin-point critical points, to switch branches at bifurcation points, and to trace critical points through parameter space. With the solver, we can explore the bifurcation landscape of the lattice metamaterial under compression and define the active nudging actuation strategy in a robust way without preknowledge of branching events. More importantly, we can trace certain critical and noncritical equilibria through parameter space directly, e.g., the size of geometric perturbation, rather than conducting expensive parameter studies. A concise and self-contained description of the FE model and the generalized path-following theory can be found in Sec. 1 of Ref. [39].

b. Passive modal nudging. Passive modal nudging [25] is a design strategy that tailors the postbuckling behavior of a load-carrying system, e.g., ultimate loading capacity, compliance and/or stability, by seeding specific geometric perturbations into the geometry that are derived from possible deformation modes of the pristine, unnudged system [as seen in Fig. 1(b)].

The procedure is based on the following steps.

(1) Explore the full bifurcation landscape of a baseline structure.

(2) Choose a desirable stable equilibrium path beyond the first instability point that does not lie on the natural path, i.e., the equilibrium path spontaneously followed by the structure upon loading, and extract the deformation mode, $\boldsymbol{u}_{\text{state}}$. Any point along said stable equilibrium path is suitable.

(3) Alter the original undeformed geometry, $\boldsymbol{x}_0$, of the baseline structure with the desired deformation mode shape, $\boldsymbol{u}_{\text{state}}$, as follows:

$$\boldsymbol{x}_{\text{nudge}} = \boldsymbol{x}_0 + \eta \bar{\boldsymbol{u}}_{\text{state}}, \tag{1}$$

where

$$\bar{\boldsymbol{u}}_{\text{state}} = \frac{\boldsymbol{u}_{\text{state}}}{\|\boldsymbol{u}_{\text{state}}\|_2}, \tag{2}$$

$$\frac{\eta \|\bar{\boldsymbol{u}}_{\text{state}}\|_2}{\|\boldsymbol{x}_0\|_2} \ll 1, \tag{3}$$

with η a nondimensional nudging parameter and $\boldsymbol{x}_0$ contains the position vector of each discretization node in the FE model.

The nudging parameter should satisfy Eq. (3) to be classified as a small geometric change. If not, the corresponding geometric alteration should not be considered a nudge, as essentially an entirely new structure with its own unique structural response is formed.

c. Active modal nudging. While passive modal nudging is used to tailor a structure's response to prescribed loading, active nudging uses secondary loading to switch between stable equilibria. Using the Roorda frame of Fig. 1 (and the symbols therein) as a reference again, the nudging process starts from an equilibrium state where the active nudging force is zero, i.e., $F_{\text{n}} = 0$, while F_{a} or u_{a} need not be 0. Under the action of F_{n}, the structure deforms away from the original equilibrium state, i.e., $F_{\text{n}} \neq 0$, while F_{a} or u_{a} remain constant depending on whether the primary loading is force or displacement controlled [displacement controlled in Fig. 1(c)]. Should F_{n} reach a separate zero, another equilibrium state would have been found, at which point active actuation would no longer be required, if said equilibrium were also stable. Similar techniques have been adopted in assessing the 'shock sensitivity' of cylindrical shells [35] and experimental path-following [36,37] to determine unstable equilibria.

A caveat for the effectiveness of active nudging is that the secondary load must have control authority [38] over the enforced deformation mode throughout the entire mode switching process, or at least in the proximity of the targeted equilibrium state.

III. BIFURCATION ANALYSIS
OF BASELINE METAMATERIAL

a. Geometry and material properties. We focus on a lattice metamaterial consisting of an elastomeric matrix with a 3 by 3 square array of circular holes. The structure is shown in Fig. 2(a). The holes have radius r and center-to-center distance a, chosen so that the initial porosity is $\phi_0 = \pi r^2/a^2 = 0.6$. The metamaterial has vertical edges broken up by columns of semicircles and strips of solid material of height $a - r$ forming straight horizontal edges. Geometric dimensions and material properties specific to the analyses herein are summarized in Table I.

Previous studies [19] explored the stability landscape of this metamaterial through experimental tests and numerical simulations but with slightly different boundary conditions.

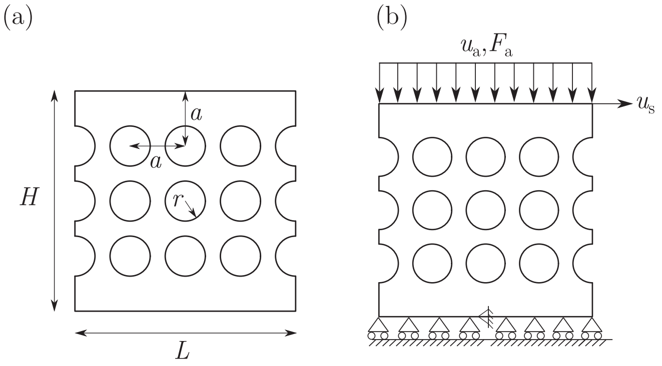

FIG. 2. (a) Geometry of finite-size metamaterial with a 3 by 3 square array of holes. Parameter a is the distance between the holes and r their radius. (b) Applied load and boundary conditions. The top edge is under uniform compression (displacement controlled loading), u_a, and can move freely in the horizontal direction with displacement u_s. The horizontal displacement at the bottom edge is restrained at the middle of the edge to prevent rigid-body motion.

Here, vertical displacements are constrained along the bottom edge, while a uniform vertical displacement u_a is applied on the top edge, as shown in Fig. 2(b). Top and bottom edges can expand or contract freely in the horizontal direction, which is different from the horizontally constraint adopted in Ref. [19]. In order to avoid rigid-body motion, the horizontal displacement of the bottom edge's mid point is assumed fixed.

b. Bifurcation diagram of baseline metamaterial. Firstly, a bifurcation analysis is conducted to explore the bifurcation landscape of the baseline metamaterial (perfect geometry). The normalized load-displacement response is presented in Fig. 3, with the stability of each equilibrium path highlighted (blue and red signify stable and unstable equilibria, respectively). The plots are presented using the nondimensional quantities $\bar{\sigma} = F_a/(L\mu)$, $\bar{\varepsilon} = u_a/H$, and $\bar{\gamma} = u_s/H$, indicative, respectively, of applied vertical load, and overall compressive and shear deformations (symbols as per Fig. 2). For clarity, abridged equilibrium paths are presented, i.e., only the fundamental path and equilibrium paths with stable equilibria are plotted. As the current finite element (FE) model cannot consider the effects of material self-contact, the analysis is terminated once self-contact occurs.

The lattice deforms almost linearly up to the pitchfork bifurcation B1. Upon branch-switching at B1, the lattice loses left–right symmetry and transitions onto one of two identical bifurcated paths, which are characterized by mirror-symmetric sheared deformation modes as shown in Fig. 3. This loading history is referred to as the *natural path*, as it describes the physical response that the metamaterial spontaneously, i.e., naturally, undergoes under the imposed compressive loading.

TABLE I. The material properties and geometric dimensions of the lattice metamaterial. Geometry parameters defined in Fig. 2(a). Dimensions as per the experimental samples manufactured and tested by Medina *et al.* [19]. Material properties are determined as per ASTM D412.

Shear modulus μ (kPa)	24
Poisson's ratio ν	0.48
Length L (mm)	50.2
Height H (mm)	50.2
Center to center distance a (mm)	12.55
Radius of holes r (mm)	5.46

In addition to these two postcritical equilibrium paths, there also exists an isolated postcritical path, corresponding to a symmetric deformation mode that becomes stable at bifurcation point B2. This isolated path is unattainable under the imposed compression loading because it is separated by an energy barrier from the fundamental path. However, it is possible to connect this isolated path with the natural loading one through modal nudging (active or passive). Both possibilities are discussed in detail in the following sections. Note that this symmetric deformation mode was also defined as *polarized* in previous research [19].

IV. TAILORING THE METAMATERIAL'S NATURAL POSTCRITICAL RESPONSE VIA PASSIVE MODAL NUDGING

Having unveiled the equilibrium manifold of the baseline metamaterial, we now aim to tailor its natural response to be biased towards the symmetric deformation mode. This is achieved by passive modal nudging, i.e., seeding a small, linearly scaled version of the symmetric deformation mode into the perfect baseline geometry. With reference to Fig. 3 to aid visualization, this nudging strategy breaks the supercritical pitchfork B1 and separates the symmetry-breaking sheared deformation modes from the symmetric deformation mode. As we aim to design a soft robot (presented hereinafter) that crawls by shape-shifting between the symmetric and asymmetric modes, in this section, focus is placed on the corresponding equilibrium manifolds. Alternatively, the baseline geometry could also be nudged with a sheared deformation mode to preferably select one mirror-symmetric sheared deformation mode over the other, i.e., to bias the metamaterial to shear left or right, but that is of less relevance to the targeted application and therefore only discussed in Sec. 3.1 of Ref. [39].

Figure 4 presents the equilibrium manifolds of the metamaterial nudged with the symmetric deformation mode. The reference state for nudging is that along the symmetric deformation mode equilibrium branch of Fig. 3 past B2 with $\bar{\varepsilon} = 0.0502$. A nudge factor η of 6.5162 is adopted. For reference, the vertical distance of the top and bottom points in the central hole decreases by 0.076 mm from the baseline metamaterial as a result of the applied nudge, which is 0.7% of the diameter of the central hole. By eroding the energy barrier that exists between the fundamental path and the isolated path of the symmetric deformation mode for the baseline metamaterial, the nudge results in a new natural loading path with deformations affine to the symmetric deformation mode, as shown in Fig. 4(b). In the advanced postbuckling regime, the new path converges asymptotically to the isolated path of the perfect baseline structure (grey curve), corresponding to the symmetric deformation mode. This happens in accordance to bifurcation theory principles owing to the shape and size of the geometric perturbation introduced in the model.

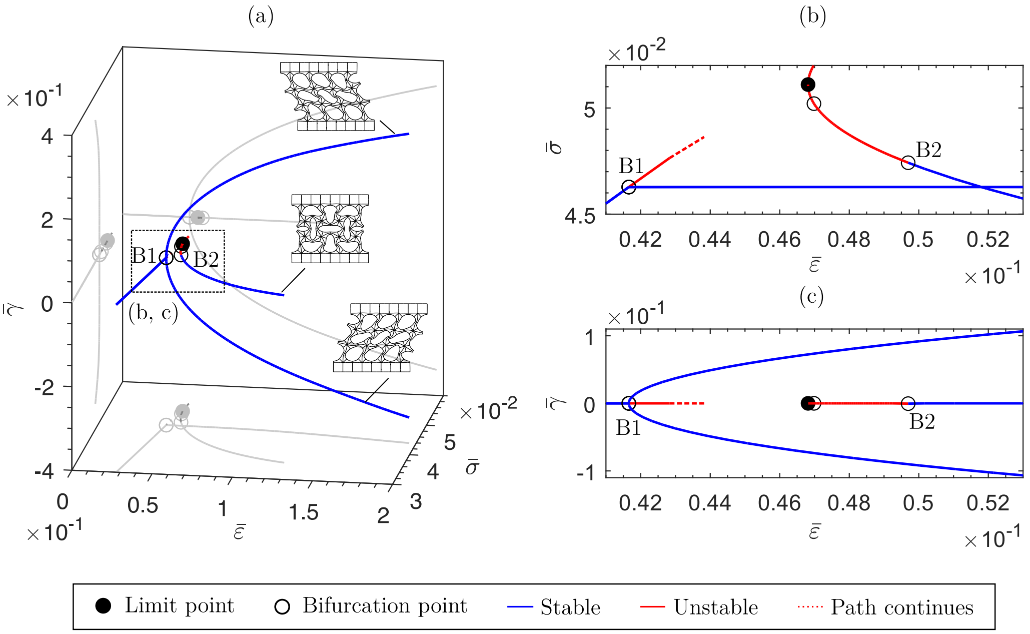

FIG. 3. Nondimensionalized load-displacement response for the lattice metamaterial with various bifurcation and limit points highlighted as hollow and solid circles, respectively. $\bar{\gamma} = u_\mathrm{s}/H$ is the normalized shear displacement at the top edge. The paths corresponding to the sheared deformation modes are disconnected from the path of the symmetric deformation mode. Bifurcation points denote intersections of equilibrium paths, while limit points are minima and maxima of the displacement applied. Note that the full stability landscape features significantly more equilibrium paths, and only the fundamental path and those leading to stable equilibria are presented here. Also shown are the deformation states at the nominal compressive strain of $\bar{\varepsilon} = 0.1$ on each path: two mirror-symmetric sheared deformation modes and a symmetric deformation mode with the central hole compressed vertically. A full bifurcation landscape can be found in Sec. 2 of Ref. [39].

There exists a threshold value of nudging required to erode this energy barrier completely. Hence, a parameter sensitivity study on the effect of the nudge factor on the bifurcation landscape is conducted, as shown in Fig. 5. The locus of the pitchfork bifurcation point B1 with respect to the nudging parameter η is traced. For illustration purposes, the equilibrium path of the baseline metamaterial is included in the figure on the $\bar{\sigma}$-$\bar{\varepsilon}$ plane. The locus of bifurcation points shows that B1 and B2 are connected in parameter space and that they converge and eventually collide at a cusp catastrophe ($\eta = 6.5162$) as the nudging parameter increases. This implies that, past the cusp, the energy barrier between the equilibrium path of the symmetric deformation mode and the fundamental path vanishes and the lattice metamaterial naturally buckles into the symmetric deformation mode. For a nudge factor smaller than the threshold value ($\eta < 6.5162$),

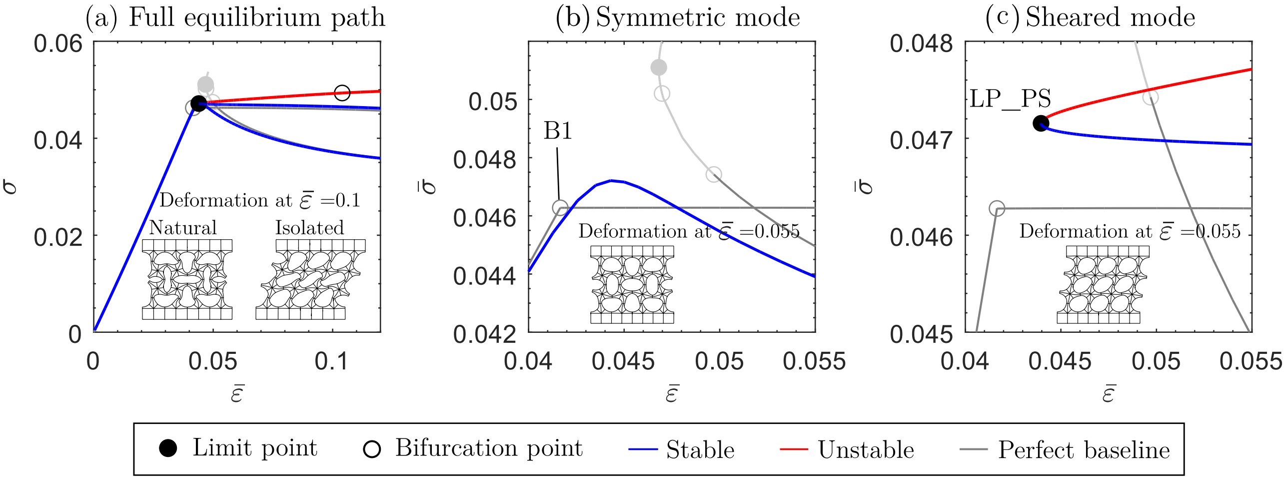

FIG. 4. Equilibrium paths and deformation profiles of the metamaterial nudged using the symmetric deformation mode. For comparison, the equilibrium path of the metamaterial with perfect geometry is also plotted in grey curves, which is identical to those shown Fig. 3(b). As shown in (b) and (c) the symmetric deformation mode is now the natural postcritical deformation mode, and both sheared deformation modes are broken-away isolated paths.

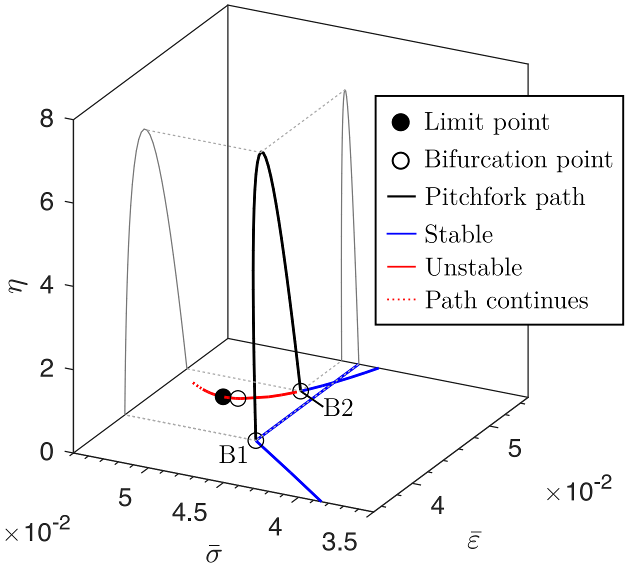

FIG. 5. Locus of bifurcation points (black curve) for different levels of nudging factor η for the symmetric deformation mode. Note that η is a nondimensional nudging parameter defined in Eq. (1), which scales the size of the geometric perturbation introduced in the structures. Above a specific nudging threshold ($\eta \geqslant 6.5162$) a cusp catstrophe is reached suggesting that the isolated branch of the baseline mode ($\eta = 0$) is now connected to the prebuckling path.

a finite energy barrier remains and the metamaterial spontaneously buckles into one of the two sheared deformation modes. In reality, a larger threshold nudging factor than determined here is required to overcome the effects arising from manufacturing imperfections (stochastic geometric imperfections and inhomogeneity of the material). More details on the effects of imperfections on the effectiveness of modal nudging can be found in Sec. 3.2 of Ref. [39].

In addition to the natural loading path, Fig. 4(c) also presents the equilibrium path of the sheared deformation mode, which in the successfully nudged scenario is now detached from the natural loading path. In the advanced postbuckling regime, the path converges to that of the sheared deformation mode of the perfect baseline structure. Note that the nudged symmetric deformation mode does not break left–right symmetry of the metamaterial. Therefore there are two mirror-symmetric sheared deformation modes as in the baseline metamaterial, and the existence of multiple stable postbuckling modes implies that we can mode switch from the symmetric deformation mode onto either sheared deformation mode by applying active nudging.

V. EXPERIMENTAL TESTING TO DEMONSTRATE PASSIVE MODAL NUDGING

To verify the effectiveness of passive nudging, we conduct a series of experiments on unnudged and nudged lattice metamaterials fabricated by molding silicone rubber. Figure 6 shows the test rig. More details on the fabrication method and testing setup are described in Sec. 6 of Ref. [39].

In manufacturing the specimens, we adopt the same planar dimensions as in Table I and a depth of $D = 40$ mm in the third dimension. The depth is comparable to the planar dimensions such that the sample does not exhibit out-of-plane buckling under the applied compression. However, the depth chosen is not sufficient to satisfy the plane strain condition (strictly speaking, infinite depth) of the 2D planar finite element models. This produces small quantitative errors between the 2D plane strain model and the experimental results. Therefore we have also conducted 3D finite element analyses in the commercial FE solver ABAQUS, which show marginally better correlation with the experimental results. Overall, the agreement between 2D plane strain model and experimental results is excellent as shown in Fig. 7.

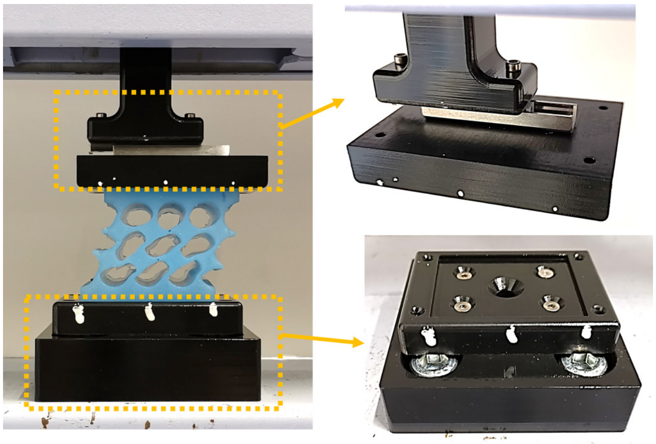

FIG. 6. Test setup for testing of the metamaterial. The top and bottom edges of the sample are partially embedded in the fixtures with a depth of 2 mm. The top fixture is connected to a smooth glide so that the top edge can move freely in the horizontal direction. The bottom fixture is fixed to the test bed of the test machine.

In the experimental campaign, three different samples were manufactured: (a) a “perfect” geometry sample, i.e., no nudge applied but background stochastic imperfections are present; (b) a passively nudged sample using the symmetric deformation mode with nudge factor below the cusp value; and (c) a passively nudged sample using the symmetric deformation mode with the nudge factor over the cusp value. Note that the symmetric deformation mode introduced is from the finite element analysis using 2D plane strain elements. All samples are first loaded into the advanced postbuckling regime with $\bar{\varepsilon} = 0.1$, to obtain the natural loading path (sheared or symmetric). Subsequently, we manually and actively nudge the samples to the other stable postbuckling mode corresponding to the respective isolated branch(symmetric or sheared) and then unload the sample to obtain the full isolated branch.

Figure 7 presents the experimental equilibrium paths of the three samples, alongside the numerical simulations from both 3D FE and 2D FE plane strain models. Each row in Fig. 7 corresponds to one sample with (a) being the pristine geometry, (b) the undernudged geometry, and (c) the successfully nudged geometry. The first and second columns denote the natural loading path [sheared for the baseline (a) and undernudged (b) geometries, and symmetric for the successfully nudged (c) geometry] with the first column showing normalized compressive force *vs* normalized compressive displacement, and the second column showing

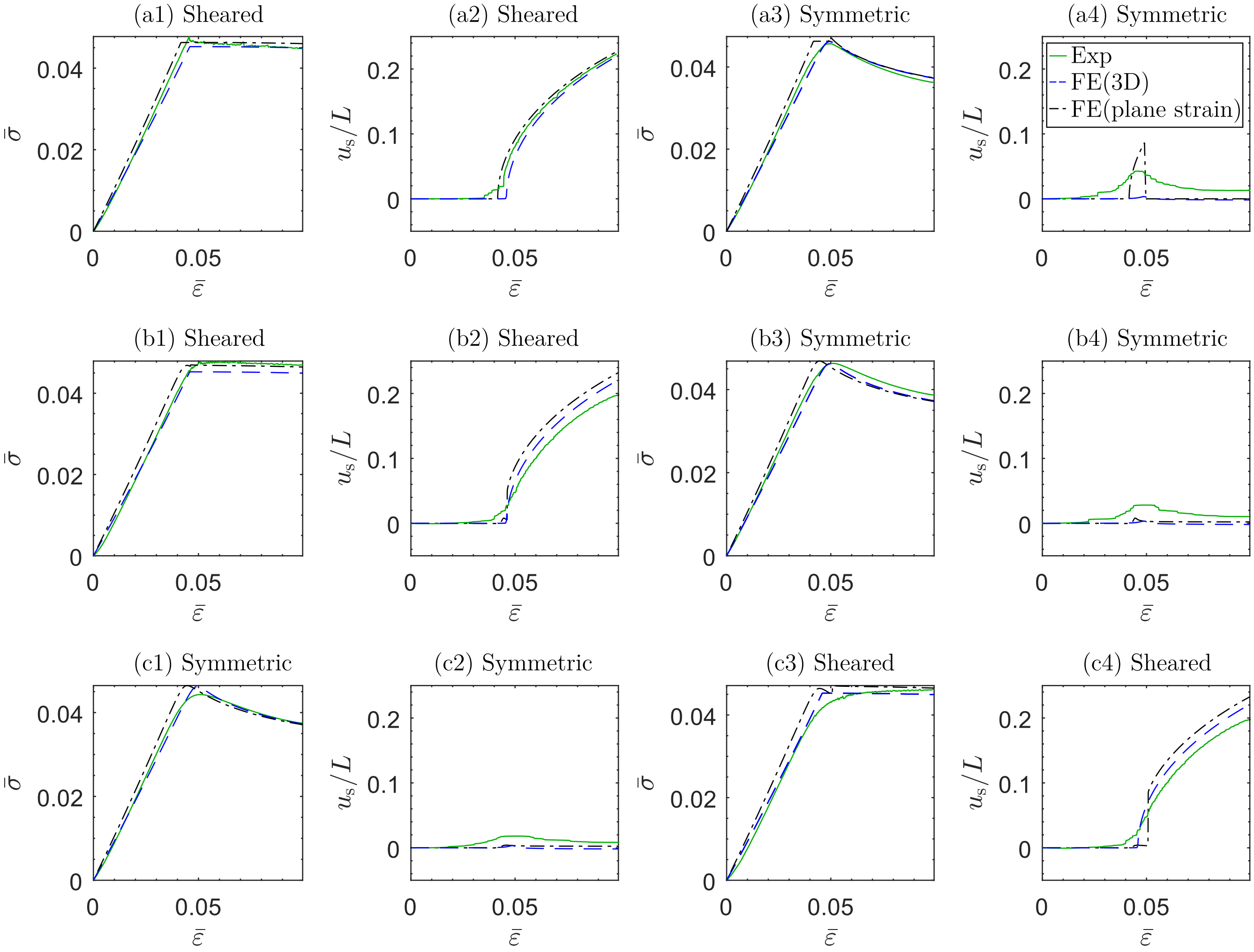

FIG. 7. Response of experimental samples with (a) baseline sample with "perfect" geometry, (b) geometrically nudged with symmetric deformation mode and nudge factor $\eta = 7.379$ (below the nudging threshold), and (c) geometrically nudged with symmetric deformation mode and nudge factor $\eta = 8.433$ (above the nudging threshold). In each case, columns 1 and 2 are the natural loading path; columns 3 and 4 are isolated paths actively nudged from the natural loading path. Columns 1 and 3 present the normalized compression force *vs* the normalized axial compression displacement at the top edge $\bar{\varepsilon}$; columns 2 and 4 present the normalized axial compression displacement $\bar{\varepsilon}$ *vs* the shear displacement at the top edge u_s/L. FE simulations using three-dimensional brick elements as well as two-dimensional plane strain elements are also shown for reference. The experimental results demonstrate successful passive nudging to the sheared and the symmetric deformation mode, i.e., successful mode selection. Videos of these tests can be seen in the video folder of Ref. [39].

normalized shearing displacement *vs* normalized compressive displacement. Columns 3 and 4 are the respective plots for the isolated branches [symmetric for (a) and (b), sheared for (c)]. Generally, both the 2D and 3D FE models compare well with the experimental results for all three samples, verifying the effectiveness of the numerical simulations. We observe some oscillations in the experimental results in the proximity of the critical point where the sheared buckling mode is triggered. Close to the critical point, the principal stiffness of the metamaterial in the direction of the buckling mode is close to zero, and therefore any misalignment in load or geometric imperfections leads to pronounced oscillations. In addition, the plots of shearing displacement, u_s, *vs* applied compressive strain, $\bar{\varepsilon}$, show a nonzero value of u_s for the symmetric deformation mode; see Figs. 7(a4), 7(b4), and 7(c2). This occurs due to the inherent stiction and friction at the top glide and eccentricities introduced during manufacturing. Note that the shear jumping in the plane strain model Fig. 7(a4) can be explained based on the bifurcation landscape of the perfect 2D plain strain model in Fig. 3(b). The nominal strain at B2, where the symmetric deformation mode loses/regains stability is larger than that at the bifurcation point B1, where shear buckling occurs. Therefore, upon unloading from symmetric, the structure will jump at B2(symmetric deformation mode) to the stable sheared deformation mode.

Both samples (a) and (b) buckle into the sheared deformation mode under the applied compressive loading. Note that the geometric nudging factor of sample (b)—the undernudged sample—is $\eta = 7.379$, which is slightly greater than the threshold for effective nudging predicted by the 2D planar model (the cusp in Fig. 5). The reasons for this discrepancy are firstly the difference between the 3D mechanics of the experimental specimen and the 2D plane strain mechanics assumed in the model, and secondly, unavoidable imperfections during manufacturing which decrease the effectiveness of a given nudge mode. Finally, sample (c) buckles into the symmetric deformation mode upon application of the compressive load, demonstrating a successfully nudged response. Indeed, increasing the nudge factor of the symmetric deformation mode, the shear component u_s in the symmetric deformation mode during the loading process decreases, as shown in Figs. 7(a4), 7(b4), and 7(c2). This reduction in shear component reflects the decaying influence of the sheared deformation mode with increasing nudging in the symmetric deformation mode.

VI. ACTIVE NUDGING THROUGH SECONDARY LOADING

The preceding sections have shown the coexistence of different stable postbuckling modes in the metamaterial under consideration, with and without passive nudges. As mentioned in the introductory sections, multistability creates the possibility for shape adaption through secondary loading. To this aim, we introduce a pair of vertical concentrated forces in the central hole, as shown in Fig. 8. An important feature of this actuation scheme is that it acts to control the local ‘microstructure’ of the metamaterial by changing the shape of the central hole: from sheared to symmetrically deformed. The choice of actuation scheme is based on a distinctive property of multistable metamaterials, that is their shape can be changed by controlling features at a smaller length scale—with smaller energy requirements—rather than the alternative strategy of mode switching by a globally applied actuation force. During active nudging, the compressive displacement at the top edge remains constant but the top edge can move freely in the horizontal direction (shear).

In this section, we navigate the nonlinear equilibrium path of the baseline metamaterial (no passive nudge). Active nudging is applied from the symmetric to the sheared deformation mode at a nominal compressive strain of $\bar{\varepsilon} = 0.0814$. The active nudging force–displacement relationship is presented in Fig. 9. Starting from the symmetric deformation mode (EP1), the lattice metamaterial deforms symmetrically on the fundamental active nudging path until this deformation mode becomes unstable at a symmetry-breaking bifurcation point NB1. The critical eigenmode of the bifurcation point is a sheared deformation mode, as shown in Fig. 9(a). Because the connected bifurcation path that branches from the bifurcation point NB1 is unstable, the metamaterial snaps dynamically into the sheared deformation mode ES0 (under force controlled loading), as shown by the dashed arrow in Fig. 9(b). With further $\bar{F}_n$ loading, the horizontal displacement of the top edge, u_s, decreases and the lattice metamaterial restores symmetry at the bifurcation point NB2, where the bifurcated path intersects with the fundamental active nudging path again. However, it is noted from Fig. 9(b) that, if the active nudging force F_n is removed at the snap-through equilibrium ES0, the metamaterial stabilizes in the equilibrium state ES1 in the form of the sheared deformation mode. Hence, we have achieved mode switching from the symmetric deformation mode (EP1) to the sheared deformation mode (ES1) by active nudging.

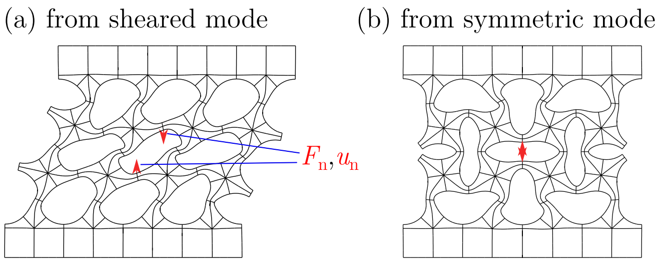
(a) from sheared mode (b) from symmetric mode

FIG. 8. Illustration of active nudging of the postbuckled metamaterial through a pair of vertical concentrated active nudging forces F_n, applied on the top and bottom edges of the central hole (red arrows). The direction of the actuation force at the top edge of the central hole is positive upwards. During active nudging, the direction of the actuation force remains vertical. The applied compressive displacement at the top edge remains constant throughout the active nudging process.

At ES1, reversing the direction of the active nudging force ($F_n < 0$), the metamaterial undergoes another snap-through instability to the symmetric deformation mode at limit point NLP1; see the dashed arrow in Fig. 9(b). When the active nudging force is removed, the metamaterial returns to the initial symmetric deformation mode EP1. In conclusion, we achieve closed-loop mode switching between sheared and symmetric deformation modes using active nudging.

The magnitude of the active nudging force required to trigger mode switching from the symmetric deformation mode to the sheared deformation mode, i.e., the force magnitude at NB1, is larger than the magnitude of the force required to mode switch from the shearing to the symmetric deformation mode, i.e., the force magnitude at NLP1. The energy input required to achieve mode switching from the symmetric deformation mode to the sheared deformation mode is also larger than the other way around. In engineering practice, it may be beneficial to make the magnitude of the active nudging force to trigger mode switching identical. This can be achieved by adjusting the compression level at the top edge, for which more details can be found in Sec. 4 of Ref. [39].

Also note that at bifurcation point NB1, the metamaterial can switch into either of the two mirror-symmetric sheared deformation modes. To make the system behave in a deterministic way, i.e., to prefer one sheared deformation mode over the other, we need to bias the metamaterial in one direction, for example, by introducing passive nudging in the shape of the sheared deformation mode. A detailed analysis on this can be found in Section 4 of Ref. [39].

VII. ACTUATION ENERGY AND FURTHER CONSIDERATIONS

a. Energy efficiency of active modal nudging. In previous work, shape-shifting in buckling-driven metamaterials was generally achieved by mode switching between the pre and postbuckling regimes [2,40], by means of loads applied on the external material boundary. In these cases, assuming no adverse effects on the shape-shifting characteristics, preloading the structure to a point in the proximity of the bifurcation can be a convenient strategy to minimize the energy input required for actuation, because, then, only a relatively small stimulus is required to trigger shape change. As shown in the

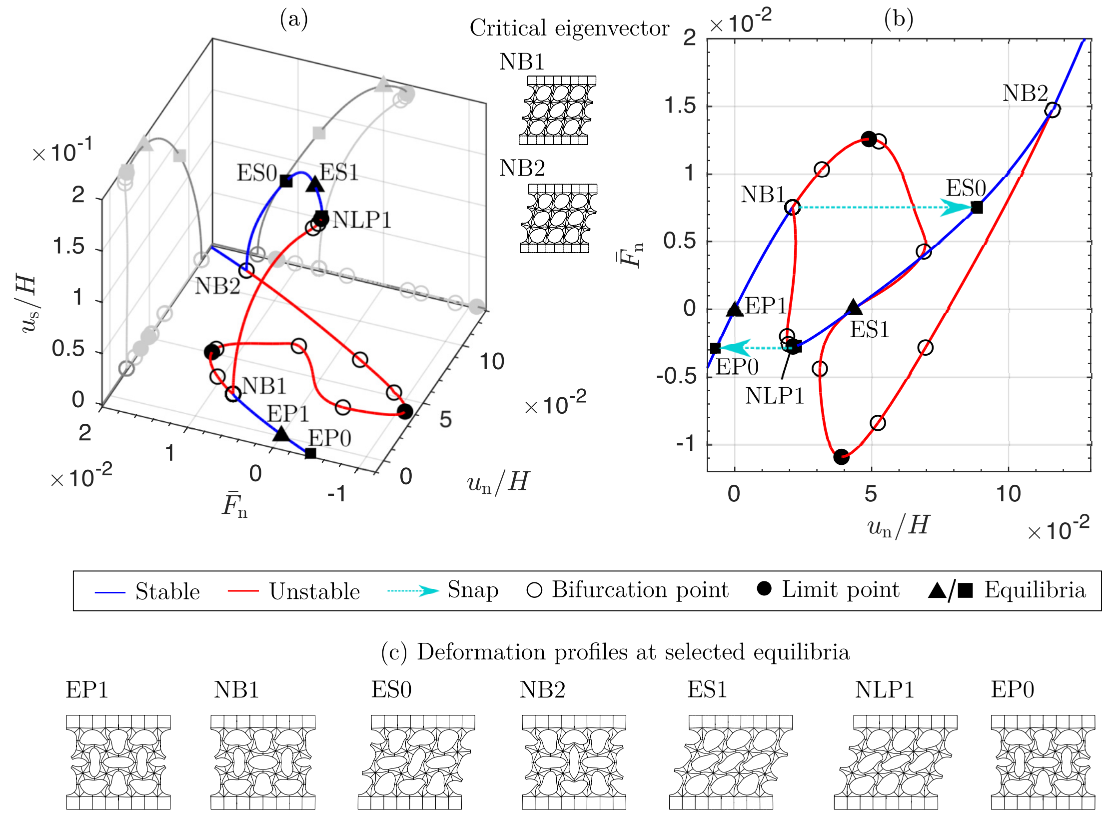

FIG. 9. Nondimensionalized active nudging force–displacement path for the baseline metamaterial without passive nudging. Also shown are the critical eigenvectors at selected bifurcation points and deformation profiles at selected equilibria. The dashed arrows in (b) represent dynamic snaps under force controlled loading due to instabilities at NB1 and NLP1. When the nudging force is removed at ES0 and EP0, the metamaterial stabilizes in the sheared deformation mode at ES1 and the symmetric deformation mode at EP1, respectively. Under the force-controlled actuation, the transition from the symmetric deformation mode to the sheared deformation mode follows the active nudging path: EP1 → NB1 → ES0→ ES1; the transition from the sheared deformation mode to the symmetric deformation mode follows the active nudging path: ES1 → NLP1 → EP0→ EP1. Note that the vertical displacement at the top edge remains $\bar{\varepsilon} = 0.0814$ through the active nudging process.

previous section, an alternative possibility is mode switching between stable postbuckling states. Further actuation energy efficiency ensues, because global shape change is triggered by local deformations, i.e., by controlling the topology at a smaller length scale.

Figure 10 compares the energy input required for shape change using these two paradigms, with actuation between pre and postbuckling states (from the symmetric unbuckled shape to the sheared deformation mode) and between postbuckling states (from the postbuckling symmetric symmetric deformation mode to the sheared deformation mode) on the left and right, respectively. For both cases, the force-displacement diagrams shown are derived from the 2D plane strain model with target shear amplitude $u_s/L = 0.20$. The energy required for actuation between pre and postbuckling states [Fig. 10(a)] is indicated by the shadowed red area subtended by the equilibrium curve. Transitioning from the bifurcation point to the targeted shear amplitude by increasing compression takes 0.227 J/m. For a fair comparison with the second actuation strategy, we neglect the energy required to load the structure up to the bifurcation point (E0 → E1), as this would only be spent once rather than cyclically for the crawling action.

For the active nudging case, the limit point and sigmoidal curve mean that actuation energy computations are more complicated as these depend on the type of actuation chosen or the loading history. With this caveat in mind, we turn our focus to an actuation scheme that balances energy efficiency and ease of implementation; that is, displacement control, maintained upon reaching the displacement limit point NDLP1, following which the structure will snap down and restabilize on sheared deformation mode ES1. The energy consumed in this case is 0.0225 J/m, i.e., 9.92% of that required with the alternative actuation method. It is, therefore, self-evident that active nudging by local actuation of an internal feature of the metamaterial is energetically more efficient than enforcing a mode change through global stimuli.

The energy required to achieve the transition from the sheared deformation mode back to the prebuckling state in Fig. 10(a) or the symmetric deformation mode in Fig. 10(b) can be calculated in a similar way. For the global actuation method, returning to the prebuckling point $u_s = 0$ is an unloading process. Therefore the corresponding energy input required is zero. For the active nudging actuation, by reversing the actuation direction, the structure will reach the displacement limit point NDLP2, following which the structure will snap up and restabilize in the symmetric deformation mode at EP1. The energy required is highlighted by the shadowed blue area, which is 0.0097 J/m in this case. Even though

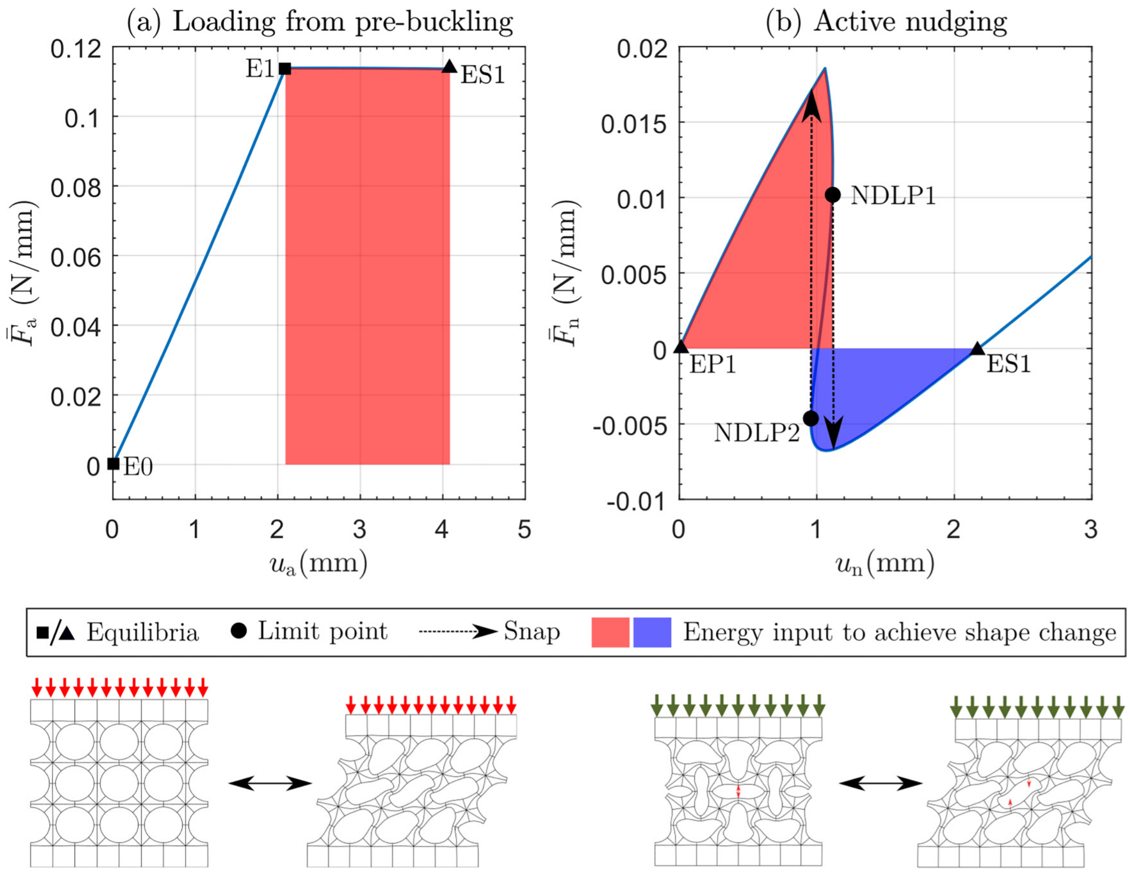

FIG. 10. The actuation force–displacement curve of the lattice metamaterial (plane strain; geometry and material properties as in Table I) to achieve a $u_s/L = 0.20$ shear displacement amplitude, using: (a) increasing compression from the prebuckling state; and (b) active nudging from the symmetric deformation mode. The red areas represent the energy input required to achieve the sheared deformation mode from the state with $u_s = 0$ [prebuckling state in (a) or the symmetric deformation mode in (b)]; the blue area represent the energy input required to achieve mode shifting from the sheared deformation mode to the symmetric deformation mode. In the deformation profiles, the red arrows represent the main actuation force applied on the lattice to achieve shape-shifting; the dark green arrows represent the constant compressive displacement. Note that the range of the vertical and horizontal axes in (b) is smaller than in (a).

in the active modal nudging process energy is input in both directions of shape-shifting, the total energy input required is only 14.21% of that required for the global actuation process. Therefore we can conclude that active nudging via local actuation is more energetically efficient if we want to use the mechanism in a repetitive manner. Note that the shadowed red and blue areas correspond to the energy barrier (under the actuation using the pair of vertical forces) between the sheared deformation mode and symmetric deformation mode.

b. Robust solver for bifurcation manifold exploration. A prerequisite for both active and passive nudging is the ability to identify most, and if possible all, stable paths in a structure's equilibrium manifold. This requires a robust path-following method that can identify equilibrium paths branching off the natural loading path, as well as isolated stable equilibria. For the former, pinpointing critical points and branch switching is sufficient. For the latter, we adopted homotopy continuation [41] based on previous knowledge of the existence and shape of isolated equilibria. In general however, in order to solve for isolated equilibria without existing knowledge of stable states, techniques such as deflated continuation would be necessary [42].

c. Effectiveness of active modal nudging. To effectively achieve active modal nudging, the actuator must exert control authority [37,43] over the metamaterial. For instance, it is not possible to achieve mode switching between the symmetric deformation mode and the sheared deformation mode through a single horizontal concentrated force applied at the top edge of the metamaterial. This force only allows mode switching between two sheared deformation modes; more details on this can be found in Sec. 4 in Ref. [39]. Therefore shape control over the central hole is an important prerequisite to achieve mode switching. In general, for nonlinear structures with more complex bifurcation landscapes and multiple stable equilibrium branches, a more systematic approach to determine the active nudging input would be required. One potential solution could be adopting a variational formulation of motion design [44] to determine the path with lowest actuation energy and the required actuation force along the path.

VIII. APPLICATION: A SOFT CRAWLING ROBOT

The previous sections have established that (1) passive nudging can be used to target one preferred postcritical mode over another throughout a loading sequence into the

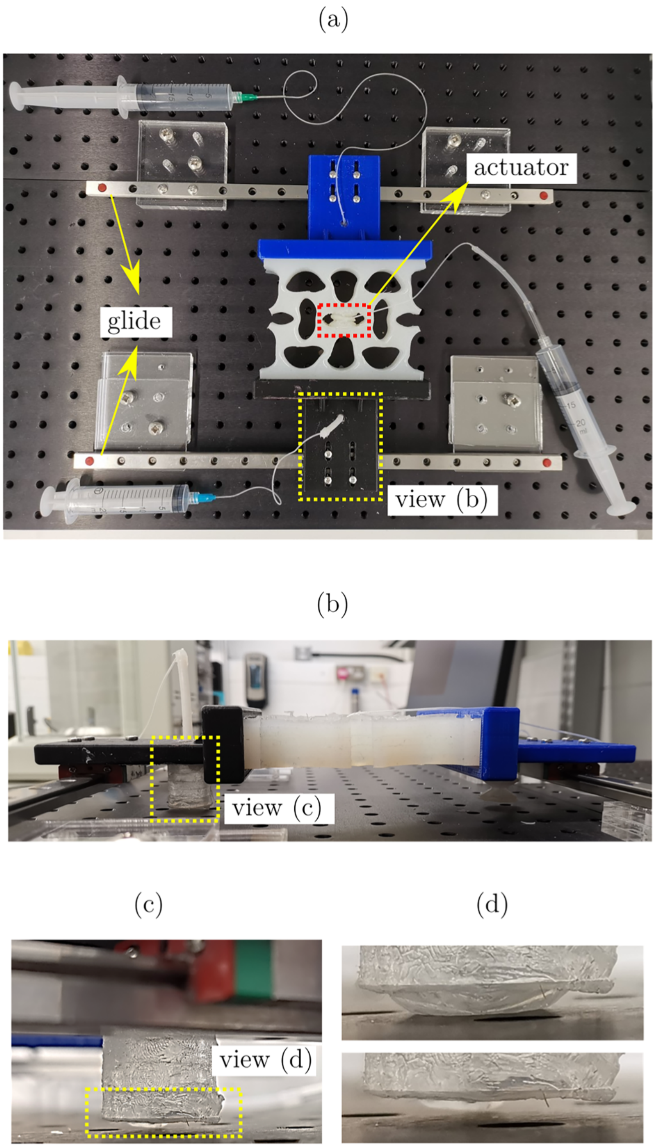

FIG. 11. [(a) and (b)] Top and side views of the crawling robot setup. The lattice metamaterial is attached to the blue and black fixtures, which are connected to carriages sitting on smooth glides. Pneumatic actuator bellows are embedded in the central hole, as well as in both fixtures. (c) Pneumatic bellow fixed onto the connector providing asymmetric friction such that the lattice metamaterial can move leftwards while mode switching between sheared and symmetric deformation modes. (d) "On" and "off" states of the bellow actuators under the fixture. The "on" and "off" states allow the carriage to be fixed or move freely on the glide.

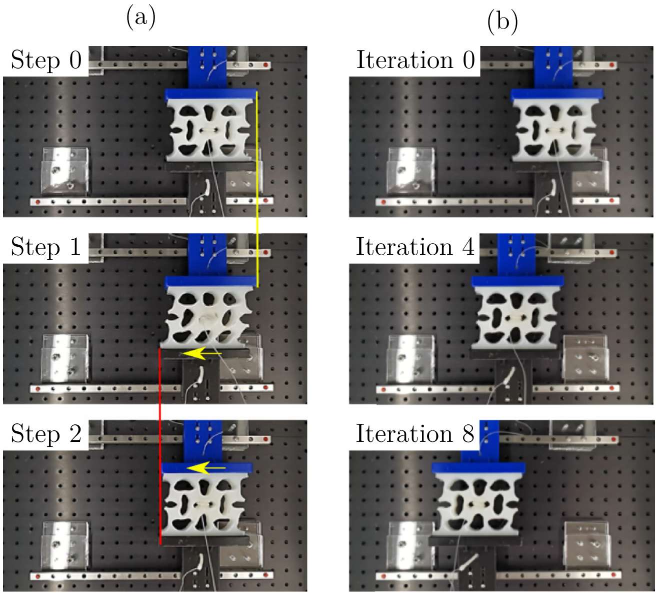

FIG. 12. (a) A typical actuation cycle for the robot. Yellow and red lines are the reference line indicating the initial and final positions of the right and left edges. The yellow arrows represent the motion of the fixture within the step. (b) The location of the crawling robot in the initial state, after four and eight iterations. A movie of the movement of the demo robot can be found in the video folder of Ref. [39].

postbuckling regime and (2) active nudging can be used to switch between different postcritical modes.

We now demonstrate the use of passive and active nudging in combination to develop a crawling soft robot; see Fig. 11. A lattice metamaterial of planar dimensions $L = 125.5$ mm and $H = 125.5$ mm (geometry shown in Table 2 scaled 2.5×) is set within two fixtures (blue and black). The vertical position of the fixtures can be adjusted to apply different levels of compression ($\bar{\varepsilon} = 0.06$ is applied herein). Said compression initially deforms the metamaterial in the symmetric deformation mode, following passive nudging to bias the natural response towards symmetry. In addition, to ensure reliable and repeatable transition to and from the symmetric and a preferred sheared deformation mode, a passive nudge affine to one of the sheared deformation modes should also be introduced upon manufacturing. However, in the present setup, this was not necessary as biased manufacturing and installation errors alongside biased friction of the glide lead to the sample preferring one sheared deformation mode over the other spontaneously.

The fixtures are connected onto carriages that can move freely on glides along the horizontal direction. Mode switching is achieved via a pneumatic bellow embedded in the central hole, which applies a pair of forces as shown in Fig. 8. To make the crawling robot move forwards, asymmetric friction mechanisms are introduced in the black and blue fixtures through additional pneumatic bellows; see Figs. 11(b) and 11(c). Figure 11(d) illustrates this mechanism. Upon pressurization of the pneumatic bellow below the black fixture, full contact with the worktop is established providing enough friction to prevent free movement along the glide; upon depressurization the bellow detaches from the worktop and the fixture can move freely again.

Figure 12(a) presents a typical actuation cycle—post application of the initial compression—where lateral movement is driven by synchronized activation of the bellow in the central hole and those under the fixtures:

Step 0: the actuators under the top (blue) and bottom (black) fixtures are "on" (inflated) and "off," respectively. The metamaterial is in the stable symmetric deformation mode.
Step 1: inflation of the central hole. The metamaterial is actively nudged into the sheared deformation mode by a snap-through instability. Since the top fixture cannot move in the horizontal direction due to friction, the bottom fixture moves leftwards.
Step 2: the status of the actuators under the top and bottom fixtures is swapped, i.e., actuators under the top and bottom fixture are, respectively, "off" and "on." The bellow in the central hole is deflated. The metamaterial undergoes snap-through and returns to the symmetric deformation mode. Since the bottom fixture is fixed in the horizontal direction and the top fixture is free to move, the top fixture moves leftwards.

By repeating the above steps cyclically, the soft robot will keep moving leftwards. Figure 12(b) shows the initial position of the robot and the positions after four and eight cycles, respectively. A movie featuring the crawling action can be found in the video folder of Ref. [39]. Note that we can also reverse locomotion in the opposite direction (moving rightwards) by swapping the sequence of actuation in the top and bottom fixtures, where the top blue fixture will move rightwards in step 1 and the bottom black fixture will move rightwards in step 2.

The soft crawling robot is controlled using the model-based open-loop strategy [45,46] or *morphological control* [47], which relies on knowledge of the nonlinear response of the lattice metamaterial to active nudging actuation based on nonlinear finite element simulations. By introducing a biased geometric perturbation in the lattice structure, the actuator can behave in a deterministic and desired manner. This approach enables the actuator to achieve the desired motion without requiring feedback control. However, as with other open-loop soft robotic systems, the main drawback is that it can only perform structured repetitive tasks that are preprogrammed in advance. In this case, the actuator is currently limited to linear locomotion. To perform more complex and unstructured tasks, the implementation of a closed-loop control system that incorporates sensors and control modules is necessary. As this is beyond the scope of the present study, it will be explored in future work.

IX. CONCLUSIONS

Although the work in this paper concerns a specific metamaterial architecture, some of the conclusions are generalizable. Namely, that the postbuckling behavior of lattice metamaterials can be programed through passive and active nudging techniques. For the metamaterial and boundary conditions considered here, there are three distinct stable postbuckling modes—two sheared deformation modes and a symmetric deformation mode. Under compressive loading, the baseline metamaterial buckles into one of the sheared deformation modes. The equilibrium path corresponding to the symmetric deformation mode is detached from the natural loading path. We demonstrate that the natural buckling response can be changed to the symmetric deformation mode using passive modal nudging, i.e., by applying a geometric perturbation affine to the symmetric deformation mode. Robust passive nudging is attained past a critical threshold magnitude of the perturbation.

In addition, we demonstrate that mode switching, in this case, between a symmetric deformation mode and a sheared deformation mode, is possible through internal (embedded) actuation, i.e., by actuation at the local length scale of the "microstructure" of the metamaterial. In the present study, this is achieved by controlling the shape of the central hole of the metamaterial. We show that shape-shifting between the sheared and symmetric postbuckling modes can be used to achieve locomotion. A demonstration crawling soft robot, exploiting both passive and active nudging is designed, manufactured and tested. Compared with traditional, globally applied actuation mechanisms, active modal nudging at the "microstructure" level is energetically more efficient.

While in this study we consider a specific type of soft metamaterial and a specific application, the design paradigms introduced can be extended to wider scenarios, such as adaptive wing structures [48,49] or facade systems [50]. As such, said paradigm has the potential to serve as a competitive means to design for energetically efficient adaptive structures.

ACKNOWLEDGMENTS

J.S. is funded by the Leverhulme Trust through a Philip Leverhulme Prize awarded to R.M.J.G. R.M.J.G. is funded by the Royal Academy of Engineering under the Research Fellowship scheme [RF \ 201718\17178].

---

[1] K. Bertoldi, P. Reis, S. Willshaw, and T. Mullin, Adv. Mater. **22**, 361 (2010).
[2] A. G. Mark, S. Palagi, T. Qiu, and P. Fischer, in *2016 IEEE International Conference on Robotics and Automation (ICRA)* (IEEE, 2016), pp. 4951–4956.
[3] Z. G. Nicolaou and A. E. Motter, Nat. Mater. **11**, 608 (2012).
[4] Q. Wang, J. A. Jackson, Q. Ge, J. B. Hopkins, C. M. Spadaccini, and N. X. Fang, Phys. Rev. Lett. **117**, 175901 (2016).
[5] X. Tan, B. Wang, Y. Yao, K. Yao, Y. Kang, S. Zhu, S. Chen, and P. Xu, Mater. Lett. **262**, 127072 (2020).
[6] A. A. Evans, J. L. Silverberg, and C. D. Santangelo, Phys. Rev. E **92**, 013205 (2015).
[7] B. Haghpanah, L. Salari-Sharif, P. Pourrajab, J. Hopkins, and L. Valdevit, Adv. Mater. **28**, 7915 (2016).
[8] A. Rafsanjani and K. Bertoldi, Phys. Rev. Lett. **118**, 084301 (2017).
[9] M. Caruel, J.-M. Allain, and L. Truskinovsky, Phys. Rev. Lett. **110**, 248103 (2013).
[10] L. Huang, Y. Duan, X. Dai, Y. Zeng, G. Ma, Y. Liu, S. Gao, and W. Zhang, Small **15**, 1902730 (2019).
[11] M. Fernandes, J. Aizenberg, J. C. Weaver, and K. Bertoldi, Nat. Mater. **20**, 237 (2021).
[12] M. Pishvar and R. Harne, Adv. Sci. **7**, 2001384 (2020).

[13] S. Li, B. Deng, A. Grinthal, A. Schneider-Yamamura, J. Kang, R. Martens, C. Zhang, J. Li, S. Yu, K. Bertoldi *et al.*, Nature (London) **592**, 386 (2021).

[14] X. Xia, C. M. Spadaccini, and J. R. Greer, Nat. Rev. Mater. **7**, 683 (2022).

[15] K. Bertoldi, V. Vitelli, J. Christensen, and M. van Hecke, Nat. Rev. Mater. **2**, 17066 (2017).

[16] S. Janbaz, M. McGuinness, and A. A. Zadpoor, Phys. Rev. Appl. **9**, 064013 (2018).

[17] A. Iniguez-Rabago, Y. Li, and J. Overvelde, Nat. Commun. **10**, 5577 (2019).

[18] S. Janbaz, F. S. L. Bobbert, M. J. Mirzaali, and A. A. Zadpoor, Mater. Horiz. **6**, 1138 (2019).

[19] E. Medina, P. E. Farrell, K. Bertoldi, and C. H. Rycroft, Phys. Rev. B **101**, 064101 (2020).

[20] T. Chen, M. Pauly, and P. Reis, Nature (London) **589**, 386 (2021).

[21] X. Ren, J. Shen, A. Ghaedizadeh, H. Tian, and Y. M. Xie, Smart Mater. Struct. **25**, 065012 (2016).

[22] X. Ren, J. Shen, P. Tran, T. D. Ngo, and Y. M. Xie, Materials and Design **139**, 336 (2018).

[23] J. Paulose, A. Meeussen, and V. Vitelli, Proc. Natl. Acad. Sci. USA **112**, 7639 (2015).

[24] P. Farrell, C. Beentjes, and Á. Birkisson, arXiv:1603.00809.

[25] B. S. Cox, R. M. J. Groh, D. Avitabile, and A. Pirrera, J. Mech. Phys. Solids **116**, 135 (2018).

[26] J. Roorda and A. H. Chilver, Int. J. Non Linear Mech. **5**, 235 (1970).

[27] R. Groh, D. Avitabile, and A. Pirrera, Comput. Methods Appl. Mech. Eng. **331**, 394 (2018).

[28] B. Haghpanah, H. Ebrahimi, D. Mousanezhad, J. Hopkins, and A. Vaziri, Adv. Eng. Mater. **18**, 643 (2016).

[29] N. Kidambi, R. L. Harne, and K.-W. Wang, Phys. Rev. E **98**, 043001 (2018).

[30] R. Groh, Comput. Methods Appl. Mech. Eng. **394**, 114839 (2022).

[31] J. Shen, A. Pirrera, and R. Groh, Proc. R. Soc. A. **478**, 20220173 (2022).

[32] G. A. H., *Nonlinear Solid Mechanics: A Continuum Approach for Engineering* (Wiley, 2000).

[33] A. Eriksson, Comput. Methods Appl. Mech. Eng. **114**, 77 (1994).

[34] E. Riks, Int. J. Solids Struct. **15**, 529 (1979).

[35] R. M. J. Groh and A. Pirrera, Proc. R. Soc. A. **475**, 20190006 (2019).

[36] R. M. Neville, R. M. J. Groh, A. Pirrera, and M. Schenk, Proc. R. Soc. A. **476**, 20190576 (2020).

[37] J. Shen, R. Groh, M. Schenk, and A. Pirrera, Int. J. Solids Struct. **210-211**, 203 (2021).

[38] R. M. Neville, R. M. J. Groh, A. Pirrera, and M. Schenk, Phys. Rev. Lett. **120**, 254101 (2018).

[39] See Supplemental Material at http://link.aps.org/supplemental/10.1103/PhysRevB.107.214103 for additional numerical results, details on experiments and fabrication, plus videos of the experiments and the soft crawling robots.

[40] D. Yang, B. Mosadegh, A. Ainla, B. Lee, F. Khashai, Z. Suo, K. Bertoldi, and G. M. Whitesides, Adv. Mater. **27**, 6323 (2015).

[41] E. Allgower and K. Georg, in *Homotopy Methods and Global Convergence* (Springer, 1983), pp. 31–42.

[42] J. Xia, P. E. Farrell, and S. G. Castro, Thin-Walled Struct. **149**, 106662 (2020).

[43] J. Shen, R. Groh, M. Schenk, and A. Pirrera, Int. J. Solids Struct. **213**, 25 (2021).

[44] R. Sachse and M. Bischoff, Int. J. Numer. Methods Eng. **122**, 972 (2021).

[45] T. George Thuruthel, Y. Ansari, E. Falotico, and C. Laschi, Soft. Robotics **5**, 149 (2018).

[46] J. Wang and A. Chortos, Advanced Intelligent Systems **4**, 2100165 (2022).

[47] E. Milana, B. Van Raemdonck, A. S. Casla, M. De Volder, D. Reynaerts, and B. Gorissen, Front. Robot. AI **8**, 413 (2022).

[48] G. Arena, R. M. J. Groh, A. Brinkmeyer, R. Theunissen, P. M. Weaver, and A. Pirrera, Proc. R. Soc. A. **473**, 20170334 (2017).

[49] E. D. Wheatcroft, J. Shen, R. M. J. Groh, A. Pirrera, and M. Schenk, Proc. R. Soc. A. **479**, 20220861 (2023).

[50] M. Khezri and K. J. R. Rasmussen, Thin-Walled Struct. **180**, 109749 (2022).